Experimental analysis of nonlinear resonances in piezoelectric plates with geometric nonlinearities

Arthur Givois · **Christophe Giraud-Audine** · **Jean-François Deü** · **Olivier Thomas**

Abstract Piezoelectric devices with integrated actuation and sensing capabilities are often used for the development of electromechanical systems. The present paper addresses experimentally the nonlinear dynamics of a fully integrated circular piezoelectric thin structure, with piezoelectric patches used for actuation and other for sensing. A phase-locked loop control system is used to measure the resonant periodic response of the system under harmonic forcing, in both its stable and unstable parts. The single-mode response around a symmetric resonance as well as the coupled response around an asymmetric resonance, involving two companion modes in 1:1 internal resonance, is accurately measured. For the latter, a particular location of the patches and additional signal processing is proposed to spatially discriminate the response of each companion mode. In addition to a hardening behavior associated with geometric nonlinearities of the plate, a softening behavior predominant at low actuation amplitudes is observed, resulting from the material piezoelectric nonlinearities.

Keywords Piezoelectric device · Nonlinear dynamics · Internal resonance · Experiments

A. Givois (✉)· O. Thomas
Arts et Metiers Institute of Technology, LISPEN, HESAM Université, 59000 Lille, France
e-mail: arthur.givois@ensam.eu

A. Givois · J.-F. Deü
Conservatoire National des Arts et Métiers, Laboratoire de Mécanique des Structures et des Systèmes Couplés (LMSSC), HESAM Université, 2 rue Conté, 75003 Paris, France

C. Giraud-Audine
Arts et Metiers Institute of Technology, University of Lille, Centrale Lille, HEI, HESAM Université, EA 2697 - L2EP - Laboratoire d'Electrotechnique et d'Electronique de Puissance, 59000 Lille, France

1 Introduction

Piezoelectric transduction is commonly used in numerous engineering applications, such as energy harvesting [1,2], micro/nano-electromechanical systems (M/NEMS) [3], and vibration control [4–6]. The transducers can be directly embedded in the mechanical structure by means of piezoelectric layers, used for both actuation and detection, obtaining a fully integrated device. This can lead to the fabrication of low-volume and portable systems. In this case, the transduction ability is of first importance [7–10].

In traditional approaches, nonlinearities are often avoided, because they lead to complex dynamical phenomena, undesirable as well as difficult to model and simulate. However, it was shown that exploiting the nonlinear behavior of electromechanical systems can help to improve their efficiency. Possible applications are energy harvesting, for which the operating frequency bandwidth can be broaden [11–14] and M/NEMS applications. In this latter context, nonlinear effects with softening or hardening behaviors around resonances (e.g., [15,16]) were observed even

at low actuation levels. They could be used to increase the amplitude range of the devices [17,18]. It was also shown that reaching nonlinear regimes can lead to decrease the phase noise [19,20], in particular by exploiting internal resonances (IRs) [21–23]. IR denotes the particular nonlinear coupling of several vibration modes of the system when their oscillation frequencies f_1, f_2 verify commensurability relations such that, among others, $f_2 \simeq f_1$ (1:1 IR), $f_2 \simeq 2f_1$ (1:2 IR), and $f_2 \simeq 3f_1$ (1:3 IR). It leads to strong exchange of energy between the modes that completely changes the topology of their forced response [24–28].

The case of a 1:3 IR with an electrostatic actuation has been addressed on numerous occasions recently: The energy exchanges between flexural modes were investigated in [29], whereas coupling between a flexural and a torsional mode was extensively studied in [21,30,31]. A 1:3 IR was also investigated on a micromachined disk resonator [32] and for a macro-piezoelectric cantilever beam [33]. More recent works reported large varieties of observed IRs in MEMS (see [34] or the review [35]). For energy harvesting applications, IRs were also explored to produce a transfer of energy toward high frequencies [36,37].

Among the different possible modal interactions, we focus here on the case of a 1:1 IR. Indeed, it appears as the simplest one since it results in the nonlinear coupling between two oscillators with close eigenfrequencies. Some mechanical systems present naturally this characteristic: two-polarized strings and beams [38–41], two-dimensional structures (rectangular/circular plates and membranes [42–44], or cylindrical shells [26,27,45,46]). The symmetry properties of plate-like structures have been identified as a promising case study. For mass sensing application, they were used in the linear regime in [47,48] to enhance the robustness of a circular diaphragm, whereas a complete procedure based on nonlinear modal interactions of a square graphene membrane was proposed in [49] to improve the sensor's sensitivity. In [50], the authors studied different 1:1 IRs between companion modes of a MEMS with a piezoelectric actuation. Another advantage of the 1:1 IR is that the different possible bifurcation scenarios are well known: The investigations [43,51,52] addressed it entirely.

Despite these numerous advantages, highlighting experimentally a 1:1 IR can be a complex operation, since no higher harmonic component is involved in the response and the two interacting modes must be separated by spatial filtering instead of frequency filtering. In [44,45,52], the coupling between companion modes of a plate was clearly identified by placing the sensors at the nodes of each mode shape. In [47,48], the authors took advantage of the rotational symmetry properties of the operational mode shapes of a circular diaphragm, to filter spatially the characteristics signal of oscillators. For this, the system was electrostatically actuated and the locations and shapes of sensing electrodes were chosen to be representative of the studied oscillators.

In line with recent investigations [52–54], a control system based on a phase-locked loop (PLL) is used to measure the geometrically nonlinear responses. A main advantage of this method is that it can measure a complete frequency response around a nonlinear mode, including its unstable parts. This method was recently used to measure nonlinear responses of MEMS [55]. However, this control method is restricted to dynamical responses with monotonous phase evolution, which can be incompatible with the emergence of an internal resonance. For instance, the complete forced responses could not be measured when an 1:1 internal resonance occurs at a location of a pitchfork bifurcation [52].

In most studies mentioned above, the internal resonances were due to geometric nonlinearities. In the case of a piezoelectric actuation and at high voltage, piezoelectric material nonlinearities were reported in [56,57], for which quadratic terms [58] and a ferroelastic hysteresis [59] in the piezoelectric constitutive law could lead to a softening behavior.

In this context, the present work focuses on the experimental investigation of the geometrically nonlinear dynamics of a fully integrated piezoelectric system at macroscale. Indeed, considering an integrated system is natural at microscale (in M/NEMS, a Duffing nonlinearity was identified in [7] and parametric excitation and amplification were, respectively, highlighted in [60] and [61]), but is scarce for macrostructures. In this paper, we address (i) the fully integrated measurement of the nonlinear frequency responses of a piezoelectric structure, (ii) the experimental investigation of a 1:1 internal resonance with an original procedure for discriminating the characteristic signals of the two oscillators, and (iii) measurements with unprecedented levels of driving voltage to ensure the activation of geometric nonlinearities.

2 The investigated piezoelectric plate

We consider an elastic circular plate (Fig. 1a) similar to one of [44,52]. Its radius and thickness are, respectively, $R = 0.11$ m and $h = 1.5$ mm. It is made of brass of mass density $\rho = 8486$ kg.m^{-3}, Young's modulus $Y = 110$ GPa, Poisson ratio $\nu = 0.3$. Eight rectangular piezoelectric patches, of dimensions $40 \times 20 \times 1$ mm, with wrapped electrodes, made of PIC 151 material, were glued on the plate with 3M Scotch-Weld DP 460 epoxy adhesive (see [62] for details about the gluing procedure). The patches are equally spaced and placed along an inner circumference or radius $r = 70$ mm. Three holes of small radius were equally spaced near the outer edge of the structure to hang up the plate with nylon threads and thus to set up experimental free edge boundary conditions (cf. Fig. 1b). A power amplifier Trek PZD700A-M/S dedicated to piezoelectric actuation enabled to amplify the voltage signals up to ± 700 V.

To verify the bonding, capacitance measurements were first performed with a standard multimeter. The capacitances $C^{(p)}$ ($p = 1, \ldots 8$) of the eight piezoelectric patches, measured between the top and bottom electrodes, were estimated at $15.85^{+1.6\%}_{-1.3\%}$ nF, showing nearly identical patches. Then, the capacitances between the bottom electrodes of the patches and the elastic plate were also measured. Values between 10 and 40 μF were obtained, about 1500 times larger than $C^{(p)}$, thus allowing to consider that all the bottom piezoelectric electrodes are at the same electric potential, because of electrostatic influence.

The particular disposition of the piezoelectric patches aimed to keep as much as possible the symmetry properties of the plate. To verify our design and to preliminary analyze the vibratory response of the plate, a modal analysis was performed from velocity measure-

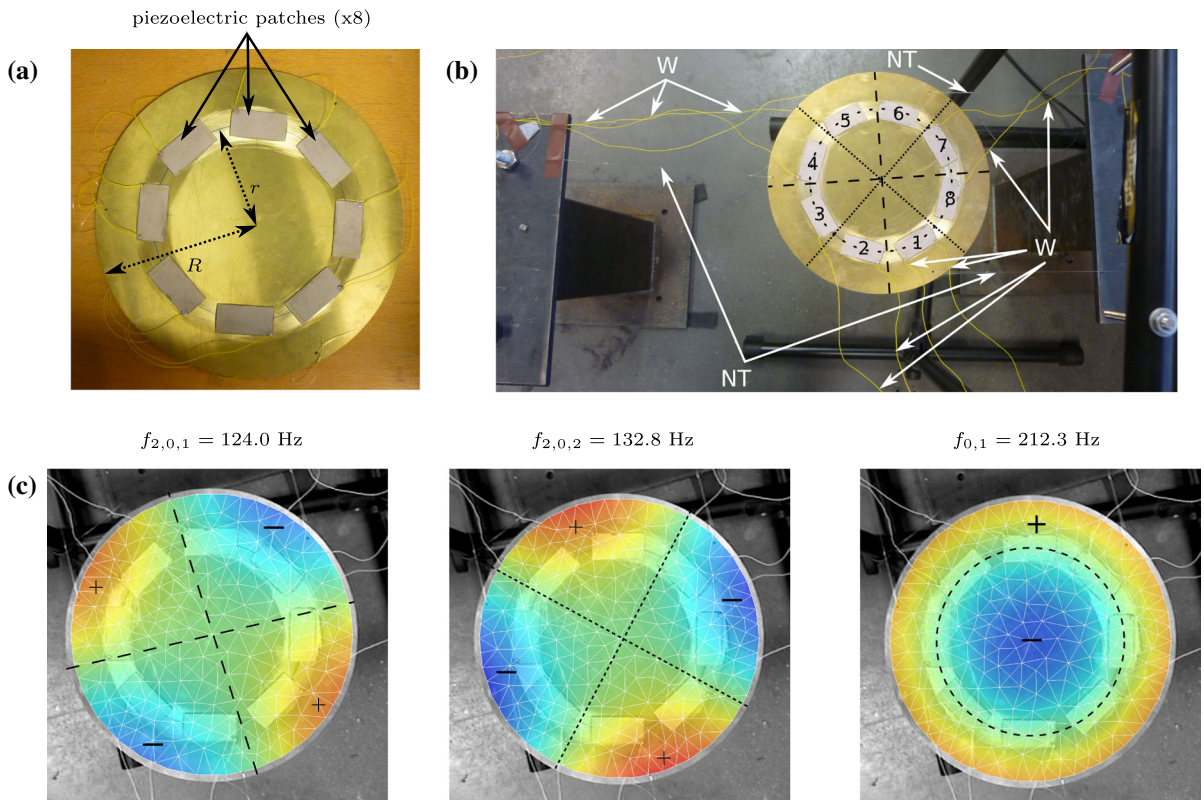

Fig. 1 Piezoelectric plate (**a**) after bonding and (**b**) in operation hanged with nylon threads (NT: nylon threads. W: elastic wires to connect the patches), (**c**) operational mode shapes of the measured modes. Nodal circles and diameters are plot in dashed lines, with different dash lengths depending on the considered mode

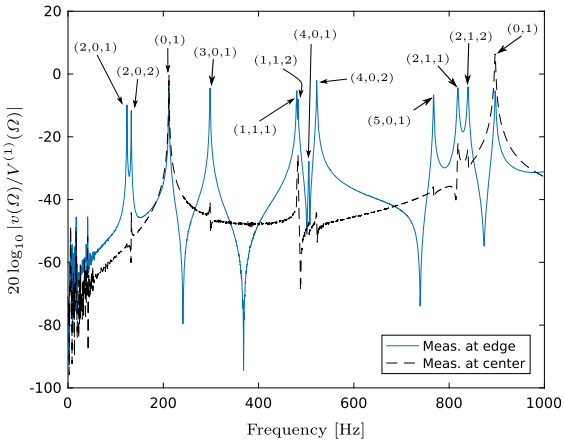

Fig. 2 Frequency response of the piezoelectric plate in velocity over voltage. The excitation voltage is prescribed at the first patch. Velocity measurements are made at a point near the edge of the plate (solid blue line) and at the center (dashed black line). Since the asymmetric modes have a node at the center of the plate, the black curve favors the emergence of the symmetric modes. The identified configurations are indicated. (Color figure online)

ments with a scanning laser vibrometer (Polytec PSV-400) and a piezoelectric driving from the first patch. Structures with a rotational symmetry are characterized by two families of modes: symmetric modes with nodal circles only and asymmetric modes with nodal diameters, the latter appearing by pairs of so-called companion modes in the spectrum. Those modes are denoted, respectively, by $(0, n)$ and $(m, n, 1)/(m, n, 2)$, with m the number of nodal diameters, n the number of nodal circles, and the last binary digit referring to the considered mode in a given pair of asymmetric companion modes. The experimental mode shapes and natural frequencies of modes (2, 0, 1), (2, 0, 2), and (0, 1), considered in the remaining of the paper, are depicted in Fig. 1c. A rotational symmetry breaking leads to a loss of equality of the two eigenfrequencies of a given companion mode pair. Figure 2 shows that the symmetry properties were kept for most of the modes of the piezoelectric plate: Indeed, most of asymmetric modes appear by pairs of modes with very closed frequencies.

3 Modeling

This section is devoted to a reduced-order model of the resonant system, including both piezoelectric transduction and geometrical nonlinearities. With this modeling, we provide a framework to predict qualitatively the dynamical resonant behavior of the system. In particular, two reduced-order models (one oscillator for a symmetric mode and two oscillators for two companion modes) will be proposed, which are mandatory to apply the experimental continuation procedure of Sects. 4 and 5.

3.1 General framework

This framework is based on the modeling proposed in [63,64], valid for any elastic structure equipped with piezoelectric patches, and taking into account both geometric nonlinearities and a linear piezoelectric constitutive law. A modal expansion on N natural modes in short circuit is used to reduce the model. Without mechanical forcing, the dynamical behavior of the structure with P patches is governed by the following equations:

$$\ddot{q}_k + 2\xi_k\omega_k\dot{q}_k + \omega_k^2 q_k + \sum_{i=1}^{N}\sum_{j=i}^{N}\beta_{ij}^k q_i q_j + \sum_{i=1}^{N}\sum_{j=i}^{N}\sum_{l=j}^{N}\gamma_{ijl}^k q_i q_j q_l + \sum_{p=1}^{P}\left[\chi_k^{(p)} + \sum_{i=1}^{N}\Theta_{ik}^{(p)} q_i\right]V^{(p)} = 0, \quad \forall k = 1,\dots N \tag{1a}$$

$$C^{(p)}V^{(p)} - Q^{(p)} - \sum_{i=1}^{N}\chi_i^{(p)} q_i - \frac{1}{2}\sum_{i=1}^{N}\sum_{j=1}^{N}\Theta_{ij}^{(p)} q_i q_j = 0, \quad \forall p = 1,\dots P. \tag{1b}$$

In these equations, $q_k(t)$ denotes the modal coordinates at time t, ω_k the natural frequencies and ξ_k the modal damping factors. $C^{(p)}$ is the capacitance of the p^{th} piezoelectric patch, measured as explained in Sect. 2. β_{ij}^k and γ_{ijl}^k are the nonlinear stiffness coefficients of the reduced-order model stemming from geometric nonlinearities, while $\chi_k^{(p)}$ and $\Theta_{ij}^{(p)}$ are the piezoelectric linear and nonlinear coupling coefficients. Finally, $(V^{(p)}, Q^{(p)})$ denotes the voltage/electric charge pair of the p-th piezoelectric

patch. Notice the $1/2$ coefficient in front of coefficients $\Theta_{ij}^{(p)}$ in Eq. (1b) [64].

3.2 One-mode reduction

In this section, we assume that the system is piezoelectrically actuated by prescribing a cosine voltage $V_a(t) = V_I \cos \Omega t$ across the terminals of the p_a-th piezoelectric patch, with its frequency Ω close to the natural frequency ω_k of one of its symmetric modes, the k-th one. The other patches are left in open circuit ($Q^{(p)} = 0$), one of them of number p_s being used as a sensor, by monitoring its voltage $V_s(t) = V^{(p_s)}(t)$. Following a normal form procedure, system (1a) can be reduced to a single oscillator with a cubic term only. The corresponding coefficient Γ_k, which embeds the effects of all quadratic and cubic coefficients $(\beta_{ij}^k, \gamma_{ijl}^k)$ of the initial system, can be explicitly obtained as a function of them, following the normal form change of coordinates (see [53,65] for details). Then, the nonlinear piezoelectric terms of coefficients $\Theta_{ik}^{(p)}$ are responsible for a parametric driving and have a significant effect only around an Arnold tongue, if $\Omega \simeq 2\omega_k$. In our study, since we are interested only in direct resonant excitation of the oscillator, with $\Omega \simeq \omega_k$, these terms are neglected. The full model thus reduces to:

$$\ddot{q}_k(t) + 2\xi_k\omega_k\dot{q}_k + \hat{\omega}_k^2 q_k(t) + \Gamma_k q_k^3 = -\chi_k^{(p_a)} V_a(t), \tag{2a}$$

$$V_s = (\chi_k^{(p_s)}/C^{(p_s)})\, q_k, \tag{2b}$$

where $\hat{\omega}_k$ is the natural frequency of the k-th mode with the p_s-th patch in short circuit and all the others in open circuit. Since the electromechanical coupling is always small, $\hat{\omega}_k \simeq \omega_k$ (see, e.g., [66]). This system has the form of a classical Duffing oscillator, driven by a force proportional to the voltage $V_a(t)$, which allows strictly applying the PLL-based nonlinear mode measurement method of [53]. Moreover, the voltage $V_s(t)$ provides a direct measurement of the modal coordinate $q_k(t)$.

3.3 Two-mode reduction

The plate is here driven by prescribing a voltage $V_a^{(p)} = V_p \cos \Omega t$ to a subset $\mathcal{P}_a \ni p$ of the patches dedicated to actuation, with the driving frequency Ω close to the natural frequencies of a pair of companion asymmetric modes. Another subset $\mathcal{P}_s$ is used for monitoring, with the patches in open circuit. To study the nonlinear dynamics of the plate, following a normal form reduction (see [43,52,65]), the modal equations (1) are reduced to a pair of oscillators, denoted by $k = 1, 2$, corresponding to the two nonlinear companion asymmetric modes, that include only cubic resonant terms:

$$\ddot{q}_1 + 2\xi_1\omega_1\dot{q}_1 + \hat{\omega}_1^2 q_1 + \Gamma_{11} q_1^3 + \Gamma_{12} q_1 q_2^2 = F_1 \tag{3a}$$

$$\ddot{q}_2 + 2\xi_2\omega_2\dot{q}_2 + \hat{\omega}_2^2 q_2 + \Gamma_{22} q_2^3 + \Gamma_{21} q_2 q_1^2 = F_2 \tag{3b}$$

$$V^{(p)} = (\chi_1^{(p)}/C^{(p)})\, q_1 + (\chi_2^{(p)}/C^{(p)}) q_2, \quad p \in \mathcal{P}_s. \tag{3c}$$

where the modal forcing reads:

$$F_1 = -\sum_{p\in\mathcal{P}_a} \chi_1^{(p)} V_a^{(p)}, \quad F_2 = -\sum_{p\in\mathcal{P}_a} \chi_2^{(p)} V_a^{(p)}. \tag{4}$$

In the above equations, in the same way than for the symmetric mode, the nonlinear piezoelectric terms are neglected and $\hat{\omega}_1$ and $\hat{\omega}_2$ are the natural frequencies of the two companion modes with the driving patches in $\mathcal{P}_a$ in short circuit and the others in open circuit. $(\Gamma_{11}, \Gamma_{12}, \Gamma_{21}, \Gamma_{22})$ denote the cubic coefficients resulting from the normal form procedure in the same manner than that was done for Eq. (2). We assumed here that only four cubic resonant terms remain, as explained in [43,52], which also present an exhaustive investigation of the obtained bifurcation scenarios. More precisely, because of the rotational symmetry, $\hat{\omega}_1 \simeq \hat{\omega}_2$ and a 1:1 IR is activated. It results in the possible emergence of a so-called elliptic mode, a particular coupled regime that involves exchanges of energy between the two oscillators that locks in a quadrature phase shift. One goal of this article is precisely to measure this coupled regime with the present fully integrated piezoelectric plate.

4 Symmetric mode measurement

This section is concerned with the nonlinear response measurement of the symmetric mode (0, 1).

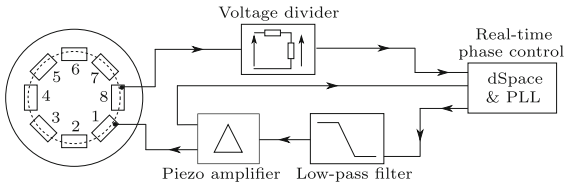

Fig. 3 Experimental setup for the symmetric mode (0, 1) measurement

4.1 Experimental setup

As introduced in Sect. 3.2 and sketched in Fig. 3, the piezoelectric plate was actuated around its first symmetric (0, 1) mode, of natural frequency 212.3 Hz, by prescribing the voltage $V^{(1)}(t) = V_a(t)$ to patch 1. Patch 8 was used for sensing, by monitoring $V_s(t) = V^{(8)}(t)$. Because of the rotational symmetry of mode shape (0, 1), any of the patches could have been used.

Following the experimental procedure described in [53], the measurements were performed thanks to the real-time control of the phase ϕ between the excitation signal $V_a(t) = V_I \cos \Omega t$ and the first harmonics of the monitoring signal $V_s(t) \simeq V_O \cos(\Omega t + \phi)$, using a dSpace MicroLabBox system with a sampling frequency $f_s = 20$ kHz. The first harmonics is estimated via a synchronous detection.

A drawback of this acquisition device is that it does not support voltage amplitudes larger than 10 V. Consequently, a voltage divider (with resistances 680 kΩ and 10 kΩ, ensuring an attenuation gain of 69) was placed at the output of the measured signals. To reduce the quantization noise generated by the digital to analog converters, a low-pass filter (a RC circuit with resistance 750 Ω and capacitance 69 nF) was placed at the output of the dSpace. The cutoff frequency was around 3 kHz, much smaller than f_s for an efficient smoothing of the output signal. For the experiments performed here, the integral and proportional gains of the control loop were, respectively, fixed at $K_I = 3$ and $K_p = 100$ (see [53] for details).

4.2 Frequency responses

Figure 4 shows the amplitudes and phases of the free and the forced responses of mode (0, 1). The free response corresponds to the backbone curve of the nonlinear mode and was obtained by prescribing a fixed value $\phi = \pi/2$ to the phase between the input and output signals of the system, and by increasing the input voltage V_I. The forced response was obtained by fixing the input voltage V_I and sweeping the phase ϕ between 0 and π. It is worth noticing that for both amplitudes and phases measurements, the experimental results are found to be outstandingly clean, for both stable and unstable parts of the curves. The result resembled to

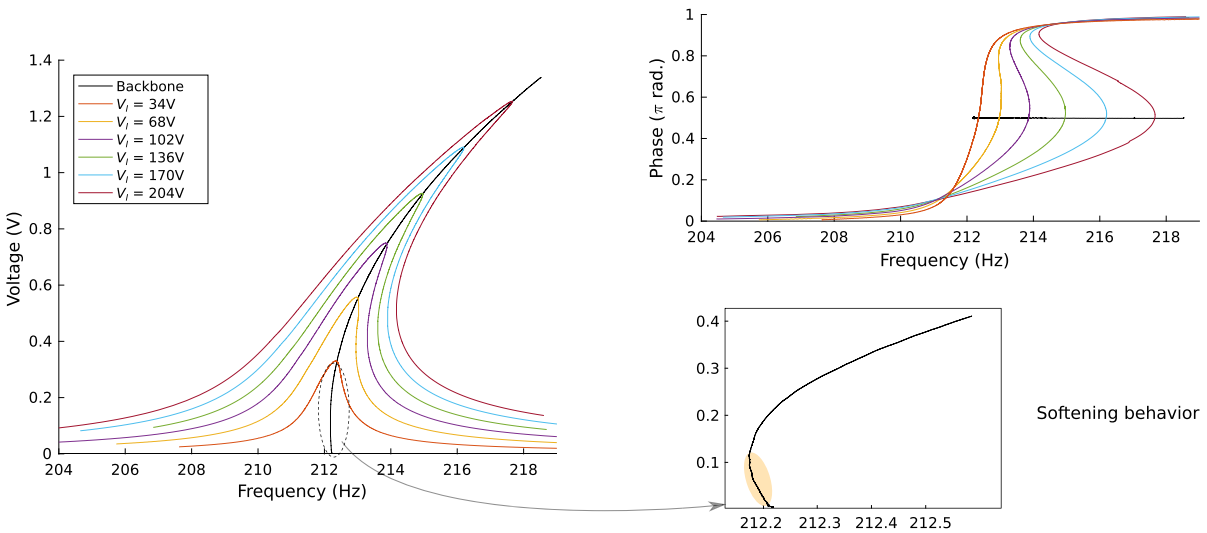

Fig. 4 Amplitudes and phases of the free (black line) and forced (colored lines) responses measured with piezoelectric detection. The input voltage is the output of the piezoelectric amplifier. Measurements are made at the output of the voltage divider. (Color figure online)

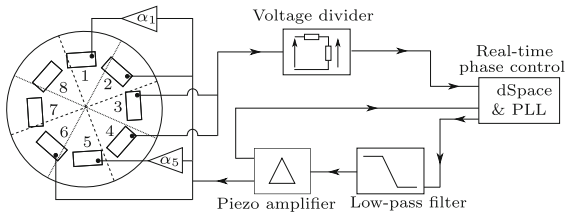

Fig. 5 Experimental setup for the asymmetric mode (2, 0) measurement

the response of a Duffing oscillator, as expected with the model of Sect. 3.2. These observations thus fully demonstrate the efficiency of the piezoelectric actuation and detection as well as the PLL control system.

As expected from nonlinear responses of an homogeneous circular plate [43,44], the nonlinear behavior of the system is mainly hardening, except at low amplitudes where a slight decrease in the frequency with the amplitude was observed. According to [59], piezoelectric material nonlinearities due to the piezoelectric patches are probably responsible for this softening nonlinearity. A reduced-order model taking into account both geometrical and piezoelectric nonlinearities would probably allow for predicting this mixed hardening–softening behavior. For this, the model of Sect. 3.2 should be corrected. A way would be to add a quadratic nonlinear term, but it would violate the normal form reduction. To remain rigorously in this framework, a fifth-order normal form reduction has to be developed, to include the change of trend of the mode, from softening to hardening. This is left out of the scope of the present study.

5 Asymmetric mode measurement

In this section, we report the measurement of the nonlinear response of the companion asymmetric modes (2, 0, 1) and (2, 0, 2).

5.1 Experimental setup

According to the modal analysis (Fig. 1c), the eigenfrequencies of the (2, 0) companion modes are located at $f_1 = 124.0$ Hz and $f_2 = 132.8$ Hz. In order to bring these two frequencies closer to favor the 1:1 IR, lests (magnets) were placed on the four nodes of the first companion mode, corresponding to antinodes of the second one, in order to significantly decrease the natural frequency of the latter without changing too much one of the former. This results in new natural frequencies of $f_1 = 122.9$ Hz and $f_2 = 124.8$ Hz, thus decreasing the frequency distance from 8.8 Hz to 1.9 Hz.

Since we are interested in properly characterizing the frequency response of the two companion modes, as it was done previously for elastic circular plates in [44,52], we want to have an experimental mean to separately actuate them and measure their respective response. As presented in Fig. 1a, c, the nodal radii of the asymmetric modes (2, 0) are not perfectly aligned with the axes of symmetry of the piezoelectric location pattern on the plate. With a theoretical perfect alignment, considering the curvature field of the deformed shapes, the coupling coefficients would have fulfilled particular equality relations such as $\chi_1^{(1)} = \chi_1^{(2)} = -\chi_1^{(3)} = -\chi_1^{(4)} = \chi_1^{(5)} = \chi_1^{(6)} = -\chi_1^{(7)} = -\chi_1^{(8)}$ and $\chi_2^{(1)} = -\chi_2^{(2)} = -\chi_2^{(3)} = \chi_2^{(4)} = \chi_2^{(5)} = -\chi_2^{(6)} = -\chi_2^{(7)} = \chi_2^{(8)}$. In this perfect case, a spatial filtering of the two companion modes, for actuation and detection, could have been obtained by simple sum and difference of the voltage signals of two neighboring patches. Due to the imperfections, this procedure was not straightforward and we had to use weighted linear combinations of the measured signals.

To separate the actuations of modes 1 and 2, we consider the electromechanical forcing $F_1(t)$ and $F_2(t)$ of the two modes in Eq. (3a, b), defined by Eq. (4). To characterize the 1:1 IR, we are interested in driving mode 1 only, thus having $F_2 = 0$. To make F_2 as small as possible, weighted linear combinations of an actuation signal were applied on two pairs of neighboring piezoelectric patches. For each pair of patches, amplifications with gains $|\alpha_p| < 1$ adjusted thanks to voltage dividers and potentiometers were applied on the driving voltage. In this setup, the actuation patches were $\mathcal{P}_a = \{1, 2, 5, 6\}$, with gains α_1 and α_5 applied to patches 1 and 5 and adjusted to minimize F_2 (see Fig. 5). By denoting the actuation voltage at the output of the amplifier as $V_a(t) = V_I \cos \Omega t$, the voltage at patches $p = 1, 5$ writes $V^{(p)} = \alpha_p V_a$, and the modal forcing reads:

$$F_1(t) = -\left(\alpha_1 \chi_1^{(1)} + \chi_1^{(2)} + \alpha_5 \chi_1^{(5)} + \chi_1^{(6)}\right) V_a(t) \tag{5a}$$

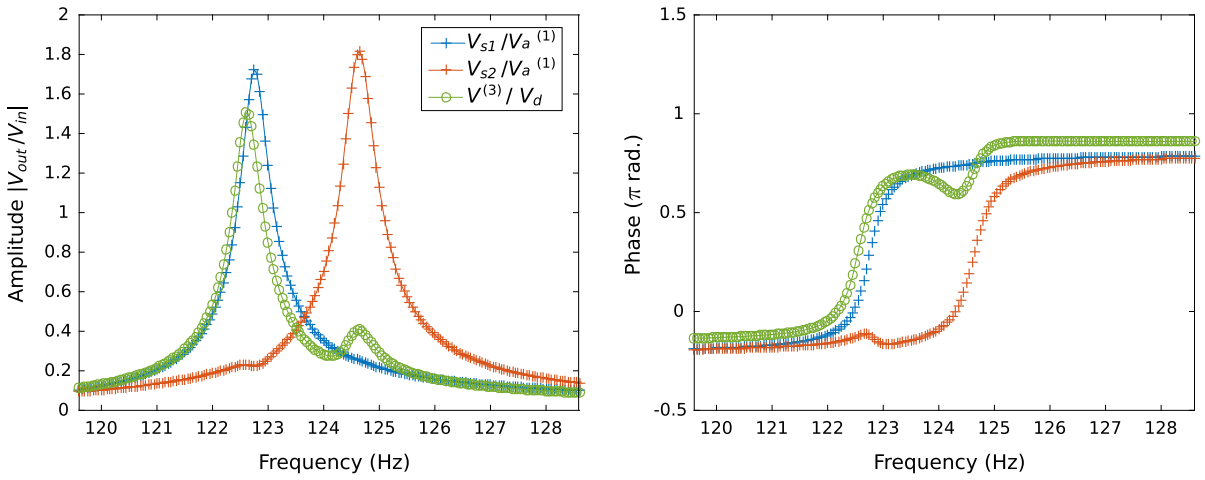

Fig. 6 Amplitudes and phases of the frequency responses for the filtering procedure. Blue and orange curves: frequency responses of measurement signals V_{s1} and V_{s2} with an actuation at patch 1. Green curve: frequency response with detection at patch 3 and prescribed voltage as described by Eq. (5). For comparison purpose, this driving signal was normalized so that $V_d = (2+\alpha^{(1)}+\alpha^{(5)})V_I$. (Color figure online)

$$F_2(t) = -\left(\alpha_1 \chi_2^{(1)} + \chi_2^{(2)} + \alpha_5 \chi_2^{(5)} + \chi_2^{(6)}\right) V_a(t) \tag{5b}$$

The sensing voltages $V^{(p)}$, governed by Eq. (3c), are recorded at patches $p = 3, 4$. For the filtering process, the combined measurements signals (V_{s1}, V_{s2}) are defined as:

$$V_{s1} = V^{(3)} + \alpha_4 V^{(4)}, \quad V_{s2} = \alpha_3 V^{(3)} + V^{(4)}. \tag{6}$$

The amplification gains α_3, α_4, applied directly in real time via the dSpace card, were adjusted such that V_{s1} and V_{s2} were, respectively, proportional to q_1 and q_2, which writes:

$$\chi_2^{(3)} + \alpha^{(4)} \chi_2^{(4)} \approx 0, \quad \alpha^{(3)} \chi_1^{(3)} + \chi_1^{(4)} \approx 0. \tag{7}$$

In practice, the gains $\alpha_i, i = 1, 3, 4, 5$, were adjusted by hand to minimize the unwanted responses of the modes, as observed in the linear frequency responses of Fig. 6. The obtained gains were $\alpha_1 = 0.7812$, $\alpha_3 = -1.83$, $\alpha_4 = 1.25$, and $\alpha_5 = 0.833$. The obtained discrimination of the companion mode was perfect for the detection since only one peak is obtained for V_{s1} and V_{s2}. For the actuation, a correct discrimination was obtained, with nevertheless a small response of mode 2, observed around 124.8 Hz, when actuating only mode 1 with the forcing pattern of Eqs. (5).

5.2 Frequency responses when driving mode (2,0,1) and 1:1 internal resonance

In the same manner as for the symmetric mode, free and forced responses were measured by the PLL system. The control was made on the phase difference ϕ_1 between the signals V_{s1} and V_a, corresponding to the actuation and sensing of mode 1, with $\phi_1 = \pi/2$ kept constant for the free response (Fig. 7) and a $\phi_1 \in [0, \pi]$ sweep for the forced response (Fig. 8).

Free responses On the basis of theoretical and experimental results reported in [52], three main characteristics in the backbone curves shown in Fig. 7 attest the emergence of a coupled regime and a 1:1 internal resonance: (i) a slight change of curvature on the amplitude response of V_{s1} around 124 Hz, characteristic of a degenerate pitchfork bifurcation; (ii) a fast increase in the amplitude of the sensing signal V_{s2} after the bifurcation; and (iii) a fast decrease in the phase of V_{s2} before the bifurcation, to reach a plateau with a phase difference close to $\pi/2$ between the two companion modes after the bifurcation. On a perfect elastic plate, the signals V_{s1} and V_{s2} would be in phase quadrature in the coupled frequency region, characteristic of the elliptic mode coupling [52]. However, probably because of the slight direct driving of mode 2 (F_2 is not zero, see Fig. 6), the amplitude of V_{s2} is not zero before the bifurcation point, leading to an imperfect coupled regime,

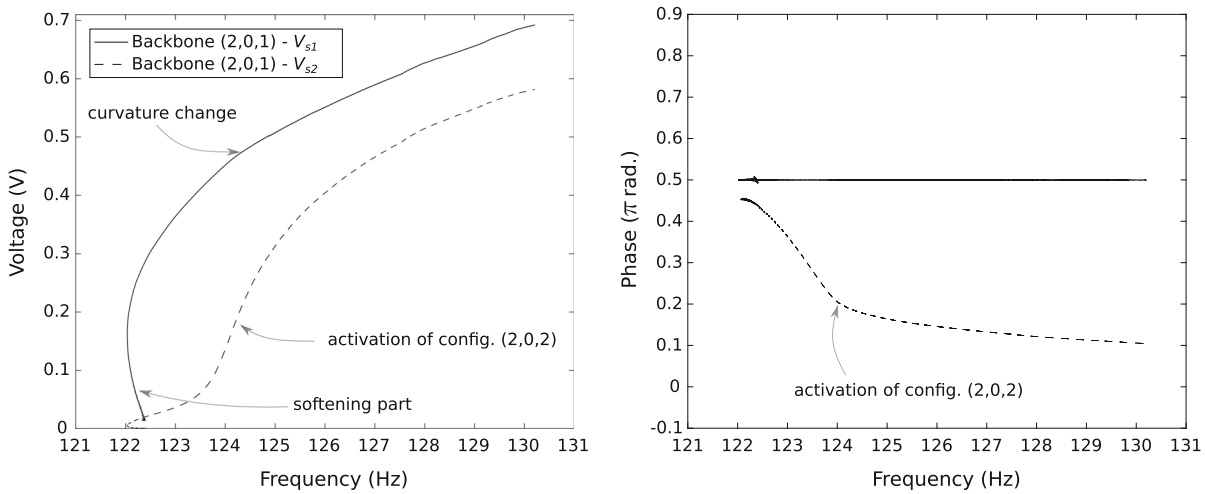

Fig. 7 Amplitudes and phases of the free frequency responses when mode (2, 0, 1) is driven. The amplitudes and phases of the signals V_{s1} and V_{s2} are, respectively, plotted with solid and dashed lines

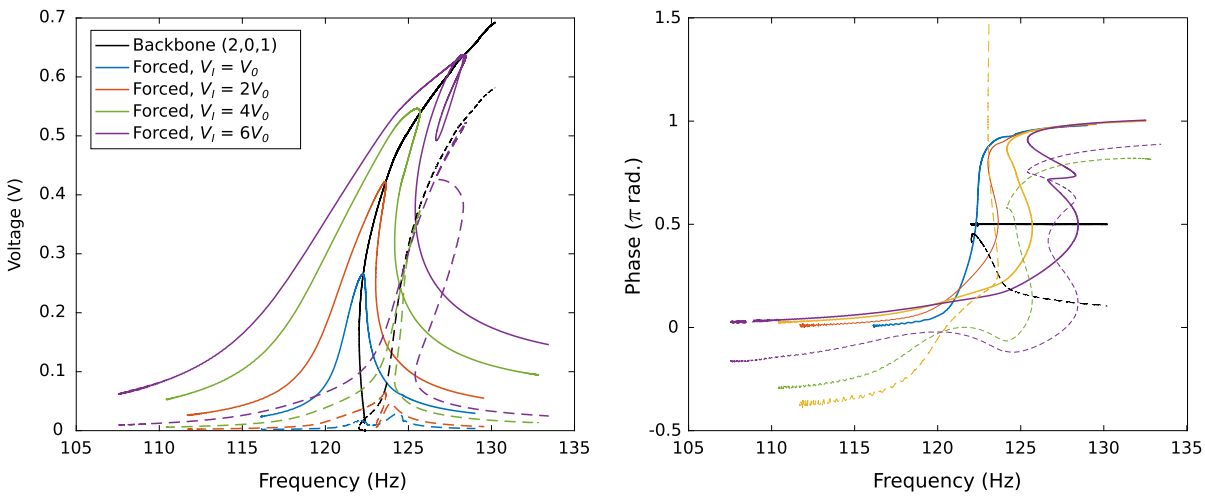

Fig. 8 Amplitudes and phases of the forced responses around the (2, 0, 1) mode, plot with colors, with $V_0 = 62$V. The amplitudes and phases of the signals V_{s1} and V_{s2} are, respectively, plotted with solid and dashed lines. The free response, plotted in black, is kept for comparison purpose. (Color figure online)

with a topology, however, very close to one of a perfect 1:1 IR.

As for the symmetric mode, a softening behavior was observed at low amplitudes. The phenomenon seemed to be more significant in the present case of the asymmetric mode than for the symmetric mode, with a larger decrease in frequency with the amplitude than the one observed in Fig. 4.

Forced responses Figure 8 depicts the forced responses for different driving amplitudes. As expected, the responses are articulated around the backbone curve, for low amplitudes where the softening behavior predominated, as well as for higher amplitudes, where geometric nonlinearities and the 1:1 IR are activated.

An unstable behavior was encountered after the phase resonances for the two higher amplitudes prescribed on the system (green and purple curves). To overcome this issue, the control gains were changed during the measurements: They were progressively increased from $K_I = 3$ and $K_p = 100$ to $K_I = 40$

and $K_p = 1000$ shortly after the phase resonance and then decreased until the end of the phase sweep. Consequently, all the curve could be measured despite the unstable behavior (unlike the experiments in [52], where controller gains were not changed), even at higher excitation levels for which a loop in the amplitude curve was encountered (cf. purple curve).

6 Conclusion

In this paper, we report original experiments on a fully integrated piezoelectric system with sufficient high actuation levels to activate geometric nonlinearities. Voltage amplitudes up to $V_I = 372$ V were applied to achieve a maximum of displacement amplitude of $w = 1$ mm. The fatigue of the piezoelectric ceramics was clearly observed during the experiment period: An inconvenient was that the upper conductive layers of all ceramics except one were broken, which could lead to the emergence of electric arcs. However, it was repaired by applying a thin graphite layer with a pencil, and no significant effect on the mechanical properties of the plate, particularly the stiffness and the resonance frequencies, was observed. The results on unimodal response measurements demonstrated the effectiveness of the PLL control system with a fully integrated piezoelectric device. An experimental procedure was set up to highlight a modal interaction between two companion modes and thus the emergence of a 1:1 internal resonance. Future developments could focus on predictive models to simulate the combined effects of piezoelectric and geometrical nonlinearities, thus allowing for the accurate comparison between theoretical calculations and experiments, and leading to the estimation of model parameters.

Acknowledgements Frédéric Guillerm is thanked for his tremendous skills in fitting and gluing piezoelectric patches.

Compliance with ethical standards

Conflict of interest The authors declare that they have no conflict of interest.

References

1. Erturk, A., Inman, D.J.: Piezoelectric energy harvesting. John Wiley and Sons, New Jersey (2011)
2. Safaei, M., Sodano, H.A., Anton, S.R.: A review of energy harvesting using piezoelectric materials: state-of-the-art a decade later (2008–2018). Smart Mater. Struct. **28**(11), 113001 (2019)
3. Trolier-McKinstry, S., Muralt, P.: Thin film piezoelectrics for MEMS. J. Electroceram. **12**(1–2), 7–17 (2004)
4. Preumont, A.: Vibration control of active structures: an introduction. Springer, Berlin (2018)
5. Gripp, J.A.B., Rade, D.A.: Vibration and noise control using shunted piezoelectric transducers: a review. Mech. Syst. Signal Process. **112**, 359–383 (2018)
6. Shivashankar, P., Gopalakrishnan, S.: Review on the use of piezoelectric materials for active vibration, noise, and flow control. Smart Mater. Struct. (2020)
7. Karabalin, R.B., Matheny, M.H., Feng, X.L., Defaÿ, E., Le Rhun, G., Marcoux, C., Hentz, S., Andreucci, P., Roukes, M.L.: Piezoelectric nanoelectromechanical resonators based on aluminum nitride thin films. Appl. Phys. Lett. **95**(10), 103111 (2009)
8. Dezest, D., Thomas, O., Mathieu, F., Mazenq, L., Soyer, C., Costecalde, J., Remiens, D., Deü, J.-F., Nicu, L.: Wafer-scale fabrication of self-actuated piezoelectric nanoelectromechanical resonators based on lead zirconate titanate (PZT). J. Micromech. Microeng. **25**(3), 035002 (2015)
9. Thomas, O., Legrand, B., Fuinel, C.: Optimization of length and thickness of smart transduction layers on beam structures for control and M, NEMS applications. In ASME: Conference on Smart Materials, p. 2015. American Society of Mechanical Engineers Digital Collection, Adaptive Structures and Intelligent Systems (2015)
10. Saya, D., Dezest, D., Welsh, A.J., Mathieu, F., Thomas, O., Leichle, T., Trolier-McKinstry, S., Nicu, L.: Piezoelectric nanoelectromechanical systems integrating microcontact printed PZT films. J. Micromech. Microeng. (2019)
11. Ramlan, R., Brennan, M.J., Mace, B.R., Kovacic, I.: Potential benefits of a non-linear stiffness in an energy harvesting device. Nonlinear Dyn. **59**(4), 545–558 (2010)
12. Daqaq, M.F., Masana, R., Erturk, A.,D Dane, Q.: On the role of nonlinearities in vibratory energy harvesting: a critical review and discussion. Appl. Mech. Rev. **66**(4) (2014)
13. Rhoads, J.F., Shaw, S.W., Turner, K.L.: Nonlinear dynamics and its applications in micro-and nanoresonators. Dyn. Syst Control Conf. **43352**, 1509–1538 (2008)
14. Soltani, P., Kerschen, G.: The nonlinear piezoelectric tuned vibration absorber. Smart Mater. Struct. **24**(7), 075015 (2015)
15. Evoy, S., Carr, D.W., Sekaric, L., Olkhovets, A., Parpia, J.M., Craighead, H.G.: Nanofabrication and electrostatic operation of single-crystal silicon paddle oscillators. J. Appl. Phys. **86**(11), 6072–6077 (1999)
16. Kozinsky, I., Postma, H.W.C., Bargatin, I., Roukes, M.L.: Tuning nonlinearity, dynamic range, and frequency of nanomechanical resonators. Appl. Phys. Lett. **88**(25), 253101 (2006)
17. Postma, H.W.C., Kozinsky, I., Husain, A., Roukes, M.L.: Dynamic range of nanotube-and nanowire-based electromechanical systems. Appl. Phys. Lett. **86**(22), 223105 (2005)
18. Tiwari, S., Candler, R.N.: Using flexural MEMS to study and exploit nonlinearities: a review. J. Micromech. Microeng. **29**(8), 083002 (2019)

19. Kenig, E., Cross, M.C., Villanueva, L.G., Karabalin, R.B., Matheny, M.H., Lifshitz, R., Roukes, M.L.: Optimal operating points of oscillators using nonlinear resonators. Phys. Rev. E **86**(5), 056207 (2012)
20. Villanueva, L.G., Kenig, E., Karabalin, R.B., Matheny, M.H., Lifshitz, R., Cross, M.C., Roukes, M.L.: Surpassing fundamental limits of oscillators using nonlinear resonators. Phys. Rev. Lett. **110**(17), 177208 (2013)
21. Antonio, D., Zanette, D.H., López, D.: Frequency stabilization in nonlinear micromechanical oscillators. Nat. Commun. **3**(1), 1–6 (2012)
22. Shoshani, O., Heywood, D., Yang, Y., Kenny, T.W., Shaw, S.W.: Phase noise reduction in an MEMS oscillator using a nonlinearly enhanced synchronization domain. J. Microelectromech. Syst. **25**(5), 870–876 (2016)
23. Cassella, C., Strachan, S., Shaw, S.W., Piazza, G.: Phase noise suppression through parametric filtering. Appl. Phys. Lett. **110**(6), 063503 (2017)
24. Nayfeh, A.H., Mook, D.T.: Nonlinear oscillations. John Wiley and sons, New-York (1979)
25. Haddow, A.G., Barr, A.D.S., Mook, D.T.: Theoretical and experimental study of modal interaction in a two-degree-of-freedom structure. J. Sound Vib. **97**(3), 451–473 (1984)
26. Thomas, O., Touzé, C., Chaigne, A.: Non-linear vibrations of free-edge thin spherical shells: modal interaction rules and 1:1:2 internal resonance. Int. J. Solids Struct. **42**(11), 3339–3373 (2005)
27. Touzé, C., Amabili, M.: Nonlinear normal modes for damped geometrically nonlinear systems: Application to reduced-order modelling of harmonically forced structures. J. Sound Vib. **298**(4–5), 958–981 (2006)
28. Monteil, M., Touzé, C., Thomas, O., Benacchio, S.: Nonlinear forced vibrations of thin structures with tuned eigenfrequencies: the cases of 1:2:4 and 1:2:2 internal resonances. Nonlinear Dyn. **75**(1), 175–200 (2014)
29. Houri, S., Hatanaka, D., Asano, M., Ohta, R., Yamaguchi, H.: Limit cycles and bifurcations in a nonlinear MEMS resonator with a 1:3 internal resonance. Appl. Phys. Lett. **114**(10), 103103 (2019)
30. Chen, C., Zanette, D.H., Czaplewski, D.A., Shaw, S., López, D.: Direct observation of coherent energy transfer in nonlinear micromechanical oscillators. Nat. Commun. **8**, 15523 (2017)
31. Czaplewski, D.A., Strachan, S., Shoshani, O., Shaw, S.W., López, D.: Bifurcation diagram and dynamic response of a MEMS resonator with a 1:3 internal resonance. Appl. Phys. Lett. **114**(25), 254104 (2019)
32. Taheri-Tehrani, P., Guerrieri, A., Defoort, M., Frangi, A., Horsley, D.A.: Mutual 3:1 subharmonic synchronization in a micromachined silicon disk resonator. Appl. Phys. Lett. **111**(18), 183505 (2017)
33. Guillot, V., Givois, A., Colin, M., Thomas, O., Savadkoohi, A.T., Lamarque, C.-H.: Theoretical and experimental investigation of a 1:3 internal resonance in a beam with piezoelectric patches. J. Vib. Control (2020)
34. Houri, S., Hatanaka, D., Asano, M., Yamaguchi, H.: Demonstration of multiple internal resonances in a microelectromechanical self-sustained oscillator. Phys. Rev. Appl. **13**(1), 014049 (2020)
35. Hajjaj, A.Z., Jaber, N., Ilyas, S., Alfosail, F.K., Younis, M.I.: Linear and nonlinear dynamics of micro and nano-resonators: Review of recent advances. Int. J. Non-Linear Mech. (2019)
36. Cao, D.X., Leadenham, S., Erturk, A.: Internal resonance for nonlinear vibration energy harvesting. Eur. Phys. J. Spec. Top. **224**(14–15), 2867–2880 (2015)
37. Xiong, L., Tang, L., Mace, B.R.: A comprehensive study of 2:1 internal-resonance-based piezoelectric vibration energy harvesting. Nonlinear Dyn. **91**(3), 1817–1834 (2018)
38. Ho, C.-H., Scott, R.A., Eisley, J.G.: Non-planar, non-linear oscillations of a beam-I. Forced motions. Int. J. Non-Linear Mech. **10**(2), 113–127 (1975)
39. Ho, C.-H., Scott, R.A., Eisley, J.G.: Non-planar, non-linear oscillations of a beam II. Free motions. J. Sound Vib. **47**(3), 333–339 (1976)
40. Thomas, O., Lazarus, A., Touzé, C.: A harmonic-based method for computing the stability of periodic oscillations of non-linear structural systems. In ASME 2010 International Design Engineering Technical Conferences and Computers and Information in Engineering Conference, volume 44137, pages 883–892. American Society of Mechanical Engineers Digital Collection (2010)
41. Vincent, P., Descombin, A., Dagher, S., Seoudi, T., Lazarus, A., Thomas, O., Ayari, A., Purcell, S.T., Perisanu, S.: Nonlinear polarization coupling in freestanding nanowire/nanotube resonators. J. Appl. Phys. **125**(4), 044302 (2019)
42. Chang, S.I., Bajaj, A.K., Krousgrill, C.M.: Non-linear vibrations and chaos in harmonically excited rectangular plates with one-to-one internal resonance. Nonlinear Dyn. **4**(5), 433–460 (1993)
43. Touzé, C., Thomas, O., Chaigne, A.: Asymmetric non-linear forced vibrations of free-edge circular plates. part 1: Theory. J. Sound Vib. **258**(4), 649–676 (2002)
44. Thomas, O., Touzé, C., Chaigne, A.: Asymmetric non-linear forced vibrations of free-edge circular plates, part 2: experiments. J. Sound Vib. **265**(5), 1075–1101 (2003)
45. Thomas, O., Touzé, C., Luminais, É.: Non-linear vibrations of free-edge thin spherical shells: experiments on a 1:1:2 internal resonance. Nonlinear Dyn. **49**(1–2), 259–284 (2007)
46. Camier, C., Touzé, C., Thomas, O.: Non-linear vibrations of imperfect free-edge circular plates and shells. Eur. J. Mech. A. Solids **28**(3), 500–515 (2009)
47. Ismail, A.K., Burdess, J.S., Harris, A.J., McNeil, C.J., Hedley, J., Chang, S.C., Suarez, G.: The principle of a MEMS circular diaphragm mass sensor. J. Micromech. Microeng. **16**, 1487–1493 (2006)
48. Ismail, A.K., Burdess, J.S., Harris, A.J., Suarez, G., Keegan, N., Spoors, J.A., Chang, S.C., McNeil, C.J., Hedley, J.: The fabrication, characterization and testing of a MEMS circular diaphragm mass sensor. J. Micromech. Microeng. **18**(2), 025021 (2008)
49. Atalaya, J., Kinaret, J.M., Isacsson, A.: Nanomechanical mass measurement using nonlinear response of a graphene membrane. Europhys. Lett. **91**(4), 48001 (2010)
50. Nathamgari, S.S.P., Dong, S., Medina, L., Moldovan, N., Rosenmann, D., Divan, R., Lopez, D., Lauhon, L.J., Espinosa, H.D.: Nonlinear mode coupling and one-to-one internal resonances in a monolayer WS_2 nanoresonator. Nano Lett. **19**(6), 4052–4059 (2019)

51. Manevitch, A.I., Manevitch, L.I.: Free oscillations in conservative and dissipative symmetric cubic two-degree-of-freedom systems with closed natural frequencies. Meccanica **38**(3), 335–348 (2003)
52. Givois, A., Tan, J.-J., Touzé, C., Thomas, O.: Backbone curves of coupled cubic oscillators in one-to-one internal resonance: bifurcation scenario, measurements and parameter identification. Meccanica **55**, 481–503 (2020)
53. Denis, V., Jossic, M., Giraud-Audine, C., Chomette, B., Renault, A., Thomas, O.: Identication of nonlinear modes using phase-locked-loop experimental continuation and normal form. Mech. Syst. Signal Process. **106**, 430–452 (2018)
54. Jossic, M., Chomette, B., Denis, V., Thomas, O., Mamou-Mani, A., Roze, D.: Effects of internal resonances in the pitch glide of chinese gongs. J. Acoust. Soc. Am. **144**(1), 431–442 (2018)
55. Taheri-Tehrani, P., Defoort, M., Horsley, D.A.: Operation of a high quality-factor gyroscope in electromechanical nonlinearities regime. J. Micromech. Microeng. **27**(7), 075015 (2017)
56. Von Wagner, U., Hagedorn, P.: Piezo-beam systems subjected to weak electric field: experiments and modelling of non-linearities. J. Sound Vib. **256**(5), 861–872 (2002)
57. Stanton, S.C., Erturk, A., Mann, B.P., Inman, D.J.: Nonlinear piezoelectricity in electroelastic energy harvesters: modeling and experimental identification. J. Appl. Phys. **108**(7), 074903 (2010)
58. Guyomar, D., Aurelle, N., Eyraud, L.: Piezoelectric ceramics nonlinear behavior. Application to Langevin transducer. J. Phys. III **7**(6), 1197–1208 (1997)
59. Leadenham, S., Erturk, A.: Unified nonlinear electroelastic dynamics of a bimorph piezoelectric cantilever for energy harvesting, sensing, and actuation. Nonlinear Dyn. **79**(3), 1727–1743 (2015)
60. Park, M., Ansari, A.: Formation, evolution, and tuning of frequency combs in microelectromechanical resonators. J. Microelectromech. Syst. **28**(3), 429–431 (2019)
61. Thomas, O., Mathieu, F., Mansfield, W., Huang, C., Trolier-McKinstry, S., Nicu, L.: Efficient parametric amplification in micro-resonators with integrated piezoelectric actuation and sensing capabilities. Appl. Phys. Lett. **102**(16), 163504 (2013)
62. Lossouarn, B., Deü, J.-F., Aucejo, M., Cunefare, K.A.: Multimodal vibration damping of a plate by piezoelectric coupling to its analogous electrical network. Smart Mater. Struct. **25**(11), 115042 (2016)
63. Lazarus, A., Thomas, O., Deü, J.-F.: Finite element reduced order models for nonlinear vibrations of piezoelectric layered beams with applications to NEMS. Finite Elem. Anal. Des. **49**(1), 35–51 (2012)
64. Givois, A.: Analyse numérique et expérimentale de vibrations non-linéaires de structures élastiques et piézoélectriques. Modèles réduits et interactions modales (Numerical and experimental analysis of nonlinear vibrations of elastic and piezoelectric structures. Reduced-order models and modal interactions). PhD thesis, HESAM Université, Paris, (in French) (2019)
65. Touzé, C., Thomas, O., Chaigne, A.: Hardening/softening behaviour in non-linear oscillations of structural systems using non-linear normal modes. J. Sound Vib. **273**(1–2), 77–101 (2004)
66. Thomas, O., Deü, J.-F., Ducarne, J.: Vibration of an elastic structure with shunted piezoelectric patches: efficient finite-element formulation and electromechanical coupling coefficients. Int. J. Numer. Methods Eng. **80**(2), 235–268 (2009)